INTERNATIONAL JOURNAL FOR NUMERICAL METHODS IN FLUIDS
Int. J. Numer. Meth. Fluids 2002; **40**:1121–1132 (DOI: 10.1002/fld.398)

Numerical investigation of the first instabilities in the differentially heated 8:1 cavity

F. Auteri[1,*,†] and N. Parolini[2]

[1] *Dipartimento di Ingegneria Aerospaziale, Politecnico di Milano, Milano, Italia*
[2] *Département de mathématiques Ecole Polytechnique Fédérale de Lausanne, Lausanne, Suisse*

SUMMARY

We present a new Galerkin–Legendre spectral projection solver for the simulation of natural convection in a differentially heated cavity. The projection method is applied to the study of the first non-stationary instabilities of the flow in a 8:1 cavity. Statistics of the periodic solution are reported for a Rayleigh number of 3.4×10^5. Moreover, we investigate the location and properties of the first Hopf bifurcation and of the three successive bifurcations. The results confirm the previous finding in the range of Rayleigh numbers investigated that the flow instabilities originate in the boundary layer on the vertical walls. A peculiar phenomenon of symmetry breaking and symmetry restoring is observed portraying the first steps of the transition to chaos for this flow. Copyright © 2002 John Wiley & Sons, Ltd.

KEY WORDS: stability of natural convection flows; bifurcations; Galerkin–Legendre spectral methods

1. INTRODUCTION

It is well known that the behaviour of flows can change dramatically as the governing parameters go through critical values at which bifurcation points are located. Recent interest in flow simulation for supercritical values of the parameters has increased the need of accurate and efficient solution methods, in order to perform the long-time simulations necessary for investigating the asymptotic behaviour of such systems. A very extensively studied example is the problem of 2D natural convection, in particular, the Rayleigh–Bénard problem and the differentially heated cavity.

In this paper we outline a new spectral solver suitable for the simulation of the time-dependent thermal convection problem. The fluid is modelled by the Boussinesq approximation, and a primitive variable formulation is employed for the Navier–Stokes equations. To achieve the desired high accuracy, the spatial discretization is based on a Galerkin–Legendre spectral method. To implement variable separation in the two spatial directions, each variable is expanded in suitable basis functions, to obtain matrices with optimally narrow bandwidth.

* Correspondence to: F. Auteri, Dipartimento di lngegneria Aerospaziale, Politecnico di Milano, v. la Masa 34, 20158 Milano, Italia.
† E-mail: auteri@aero.polimi.it

Received 31 December 2001
Revised 1 July 2002

A second-order incremental projection method [1] is adopted to discretize in time the equation system governing velocity, pressure and temperature fields according to a three-level BDF scheme [2].

The accuracy of the proposed method is assessed by a test against a known analytical solution and by comparison with benchmark results for the problem of natural convection in a square differentially heated cavity. We also provide efficiency tests on scalar and vectorial architectures.

The spectral method is then applied to the investigation of the thermal convection flow in a differentially heated rectangular cavity. For this problem extensive studies of the instability mechanisms and of the chaotic behaviour have been made by several authors, see e.g. References [3, 4]. We consider a cavity with height to width aspect ratio of 8, filled by a fluid with $Pr=0.71$, at high, supercritical, Rayleigh numbers, $Ra>3\times10^5$. The details concerning the problem definition are not reported here for the sake of conciseness, a thorough description of the problem, including the governing equations, non-dimensional scaling and boundary conditions can be found in Reference [5]. We investigate the dependency of the solution properties on the spatial resolution adopted for $Ra=3.4\times10^5$. Afterwards, we concentrate on the investigation of the first instabilities that occur in the flow. In particular, we find that the first instability is a Hopf bifurcation closely followed by several (we counted three) transcritical instabilities which alternatively break and restore the skew-symmetry of the flow.

The paper is organized as follows. In Section 2 we briefly outline the numerical procedure and report numerical tests which assess the accuracy, in time and space, and efficiency of the method. In Section 3, we present the numerical results for the 8:1 differentially heated cavity problem.

2. NUMERICAL METHOD

2.1. Galerkin–Legendre spectral approximation

A distinctive feature of the proposed method is that appropriate bases are adopted for the approximation of the different unknowns. In particular, for the velocity we adopt a basis proposed by Shen [6] (here referred to as L_n^*) in both spatial directions, and, for the pressure, the orthogonal Legendre polynomials L_n, suitably scaled to obtain a mass matrix equal to the identity ($L_n^\diamond$). For the temperature approximation, we adopt two different bases to match the different boundary conditions in the two directions. The L_n^* basis is employed in the x-direction, where Dirichlet boundary conditions are imposed, while a different basis ($L_n^\star$) is employed in the y-direction to impose Neumann boundary conditions in an essential way. Hence, we have the following double expansions for the discrete variables:

$$\boldsymbol{u}_{n,m}(t,x,y)=\sum_{n=0}^{N}\sum_{m=0}^{M}\boldsymbol{U}_{n,m}(t)L_n^*(x)L_m^*(y) \tag{1}$$

$$p_{n,m}(t,x,y)=\sum_{n=0}^{N-2}\sum_{m=0}^{M-2}P_{n,m}(t)L_n^\diamond(x)L_m^\diamond(y) \tag{2}$$

$$\theta_{n,m}(t,x,y)=\sum_{n=0}^{N}\sum_{m=0}^{M}\Theta_{n,m}(t)L_n^*(x)L_m^\star(y) \tag{3}$$

These choices allow us to fully exploit variable separation in the resulting algorithm and minimize the bandwidth of the discrete operators.

2.2. Second-order incremental projection method

The system of the Navier–Stokes equations for a Boussinesq fluid is discretized in time by a second-order BDF scheme. The equations of the system are uncoupled by the incremental projection method of Guermond and Quartapelle [1] whose spectral implementation according to the BDF scheme analysed in Reference [2] is described in Reference [7] in the context of a Galerkin–Legendre spectral approximation.

A particular feature of this projection method is that the end-of-step, divergence free, velocity is completely eliminated from the algorithm thanks to the fact that the intermediate velocity converges to the exact solution with the same order of accuracy [1], see also Reference [7].

The non-linear and temperature terms in the momentum equation and the advection term in the temperature equation are taken into account explicitly by introducing the extrapolations $\boldsymbol{u}_\star^{k+1} \equiv 2\boldsymbol{u}^k - \boldsymbol{u}^{k-1}$ and $\theta_\star^{k+1} \equiv 2\theta^k - \theta^{k-1}$ for the velocity and temperature, respectively. As a result, we obtain the following cascade of discrete elliptic problems: first, solve the diffusion step provided by the BDF time discretization

$$\begin{cases} \dfrac{3\boldsymbol{u}^{k+1} - 4\boldsymbol{u}^k + \boldsymbol{u}^{k-1}}{2\Delta t} - \sqrt{\dfrac{Pr}{Ra}}\nabla^2\boldsymbol{u}^{k+1} = -(\boldsymbol{u}_\star^{k+1} \cdot \boldsymbol{\nabla})\boldsymbol{u}_\star^{k+1} \\ -\frac{1}{3}\boldsymbol{\nabla}(7p^k - 5p^{k-1} + p^{k-2}) + \hat{\boldsymbol{\jmath}}\theta_\star^{k+1} \\ \boldsymbol{u}^{k+1}|_{\partial\Omega} = 0 \end{cases} \tag{4}$$

then, perform the projection step formulated as Poisson problem for the pressure increment $(p^{k+1} - p^k)$

$$-\hat{\nabla}^2(p^{k+1} - p^k) = -\frac{3}{2\Delta t}\boldsymbol{\nabla} \cdot \boldsymbol{u}^{k+1}, \quad \frac{\partial(p^{k+1} - p^k)}{\partial n}_{|\partial\Omega} = 0 \tag{5}$$

finally, solve for the temperature

$$\begin{cases} \dfrac{3\theta^{k+1} - 4\theta^k + \theta^{k-1}}{2\Delta t} - \dfrac{1}{\sqrt{Ra\,Pr}}\nabla^2\theta^{k+1} = -\boldsymbol{u}^{k+1} \cdot \nabla\theta_\star^{k+1} \\ \theta^{k+1}|_{x=\pm W/2} = \mp\frac{1}{2}, \quad (\partial\theta^{k+1}/\partial n)|_{y=\pm H/2} = 0 \end{cases} \tag{6}$$

2.3. Algebraic problem

The time and space discretizations lead to the final algebraic problem, which can be written in the following compact matrix form:

$$\boldsymbol{U}^{k+1}N^* + M^*\boldsymbol{U}^{k+1} + \gamma M^*\boldsymbol{U}^{k+1}N^* = \boldsymbol{F}^{k+1} \tag{7}$$

$$D^\diamond(P^{k+1} - P^k) + (P^{k+1} - P^k)E^\diamond = G^{k+1} \tag{8}$$

$$\Theta^{k+1}N^\star + M^*\Theta^{k+1} + \chi M^*\Theta^{k+1}N^\star = H^{k+1} \tag{9}$$

where $\gamma = 3/(2\Delta t)\sqrt{Pr/Ra}$ and $\chi = 3/(2\Delta t\sqrt{Ra\,Pr})$. M and N are the mass matrices in the x- and y-direction, respectively, while $D^{\diamond}$ and $E^{\diamond}$ are the stiffness matrices. The non-linear term of the momentum equation and its counterpart in the temperature equation are evaluated by means of the pseudospectral technique based on the Gauss–Legendre quadrature with $\frac{3}{2}N$ points, to ensure exact integration of the quadratic non-linearities. The solutions of the algebraic systems (7) for the two velocity components and (9) for the temperature are obtained by means of direct fast Helmholtz solvers based on the eigendecomposition of the mass matrices in the two spatial directions. The solution of the pressure system (9) is obtained by an analogous fast spectral Poisson solver which is based on the eigendecomposition of the stiffness matrices.

2.4. Accuracy and performance evaluation

The accuracy of the proposed method has been evaluated both by investigating the rate of convergence, in space and time, and by comparison with benchmark results available in the literature.

For the analytical test case, the following unsteady exact solution of the Boussinesq equations in a $[-1,1]^2$ square domain has been employed:

$$\begin{aligned} u &= -\cos(\pi x)\sin(\pi y)\sin(2t) \\ v &= \sin(\pi x)\cos(\pi y)\sin(2t) \\ p &= -\tfrac{1}{4}\,[\cos(2\pi x)+\cos(2\pi y)][\sin(2t)]^2 \\ \theta &= \cos(\pi x)\cos(\pi y)\sin(2t) \end{aligned} \tag{10}$$

corresponding to the forcing terms

$$\begin{aligned} f_u &= -\cos(\pi x)\sin(\pi y)[2\cos(2t)+2\pi^2(Ra/Pr)^{-1/2}\sin(2t)] \\ f_v &= \sin(\pi x)\cos(\pi y)[2\cos(2t)+2\pi^2(Ra/Pr)^{-1/2}\sin(2t)] - \cos(\pi x)\cos(\pi y)\sin(2t) \\ f_\theta &= \cos(\pi x)\cos(\pi y)[2\cos(2t)+2\pi^2(Ra\,Pr)^{-1/2}\sin(2t)] \end{aligned} \tag{11}$$

with an obvious meaning of the symbols. To test space convergence, the same solution but without time dependence has been employed.

As shown in Figure 1, where the $l^{\infty}(L^2(\Omega);0,T)$ norm of the error is plotted, the method is second order accurate in time and converges with spectral accuracy in space.

To further test the accuracy of the proposed method, we compared present results for the problem of the differentially heated square cavity with the benchmark proposed by Le Quéré [8]. The comparison reported in Table I clearly shows the high accuracy of the method.

The performance of the method has been evaluated for the 8:1 differentially heated cavity problem. The CPU time per degree of freedom and time step has been determined for two

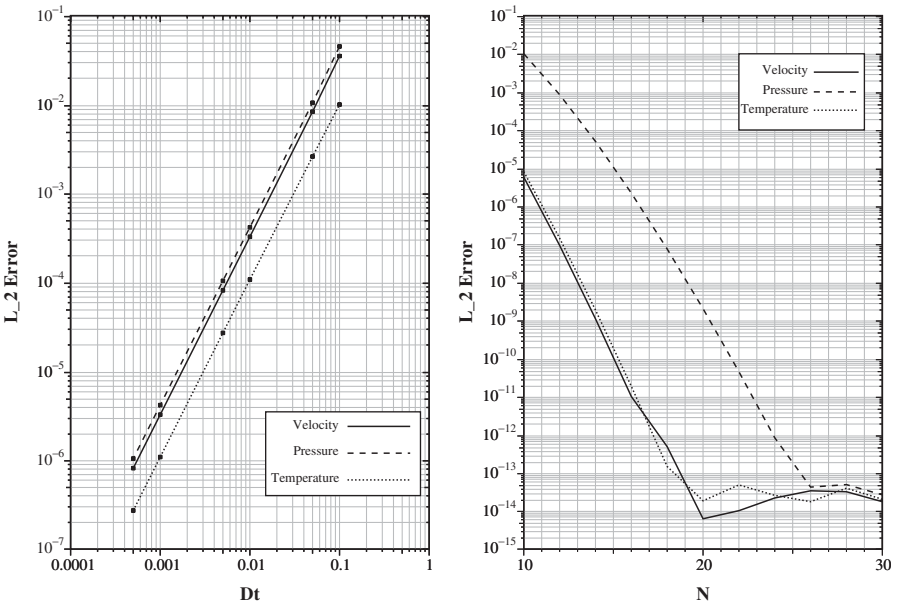

Figure 1. Convergence plot for the analytical test case. (Left) Error in $l^{\infty}(L^2(\Omega);0,T)$ norm versus Δt. (Right) Error in $L^2(\Omega)$ norm versus polynomial degree, a linear behaviour indicates a spectral convergence on this semi-logarithmic scale.

Table I. Differentially heated square cavity at $Ra=1.4085\times10^6$: comparison between the present results and benchmark results in Reference [8], where a different non-dimensionalization has been adopted so that $Ra=10^6$ therein. N polynomial degree in both dimensions, ψ_{mid} stream function in the centre of the cavity, $u_{\max}$ maximum horizontal velocity on the vertical midline, y vertical position of $u_{\max}$, $v_{\max}$ maximum vertical velocity on the horizontal midline, x horizontal position of $v_{\max}$.

	N	$\psi_{\text{mid}}\times10^2$	$u_{\max}\times10^2$	y	$v_{\max}\times10$	x	$Nu_{x=0}$
Present	32	−1.63864	6.48340	0.850	2.2057	0.038	8.8244
	48	−1.63864	6.48344	0.850	2.2057	0.038	8.8252
	64	−1.63864	6.48344	0.850	2.2057	0.038	8.8252
	72	−1.63864	6.48344	0.850	2.2057	0.038	8.8252
Le Quéré [8]	32	−1.63868	6.48351	0.850	2.2056	0.038	8.8252
	48	−1.63864	6.48338	0.850	2.2058	0.038	8.8252
	64	−1.63864	6.48343	0.850	2.2059	0.038	8.8252
	72	−1.63864	6.48344	0.850	2.2059	0.038	8.8252

distinct architectures, namely a scalar entry level workstation, a Digital Alpha 433*au*, and a vector NEC SX-5 supercomputer; the precise specifications of the two machines together with the result of the performance test are reported in Table II. Such results assess the efficiency of the method.

Table II. Employed computational resources and obtained performance for the 8:1 cavity test.

Machine		Digital 433*au*	NEC SX-5
Clock rate (MHz)		433	250
Total memory (Mbytes)		128	32768
Peak FLOP rate (MFLOPs)		866	8192
Number of processors		1 of 1	1 of 6
CPU time/d.o.f/time step (s/d.o.f./step)	20×80	6.43×10^{-5}	9.37×10^{-6}
	30×120	8.99×10^{-5}	8.60×10^{-6}
	40×160	1.22×10^{-4}	1.08×10^{-5}
Memory used (Mbytes)	20×80	3.1	3.1
	30×120	5.8	5.8
	40×160	9.6	9.6

3. RESULTS

In this section, numerical results obtained for the differentially heated 8:1 cavity are reported, see Reference [5] for an exhaustive description of the problem. Since our algorithm is symmetry preserving, i.e. the symmetry properties of the IBVP are preserved during the simulation, the initial condition used in all the reported simulations is the fluid at rest and a randomly distributed temperature with a maximal amplitude of about one-tenth of the temperature difference between the vertical walls. This allows us to observe skew-symmetry breaking instabilities that it would have been impossible to observe starting from a skew-symmetric temperature field in a quiescent fluid.

3.1. Solution at $Ra = 3.4 \times 10^5$

As a first case, we considered the flow for $Pr = 0.71$ and $Ra = 3.4 \times 10^5$ as proposed in Reference [5]. To verify the solution accuracy at this relatively high Rayleigh number, four different spatial resolutions have been considered, employing 20×80, 30×120, 40×160 and 50×200 polynomials in the horizontal and vertical directions, respectively. Once an asymptotic solution has been obtained for the coarser discretization, this solution has been used as starting point for the finer simulation. The coarsest, simulation has been run for 1 000 000 time steps with $\Delta t = 10^{-3}$ while the others for 500 000 time steps with the same Δt.

For all the discretizations, the final asymptotic solution displays a periodic asymptotic behaviour, as expected for such parameter value. Figure 2 contains four snapshots of the fluctuating contribution to the temperature field evolving in one period. In Figure 3(right) the periodic time history of the temperature in the point of co-ordinates $(0.181, 7.370)$ is shown. In Tables III and IV we report the results concerning the four space discretizations. In particular, we present the average value and oscillation amplitude of the velocity components u and v, temperature θ, stream function ψ and vorticity ω, at point $(0.181, 7.370)$; moreover, we present the Nusselt number on the two vertical walls $Nu_{x=0}$ and $Nu_{x=W}$, the total kinetic energy $\hat{u}$, the enstrophy $\hat{\omega}$ and the oscillation period T for all the aforementioned quantities. We report also the skewness ε, defined by $\theta(0.181, 7.37) + \theta(0.819, 0.63)$, which

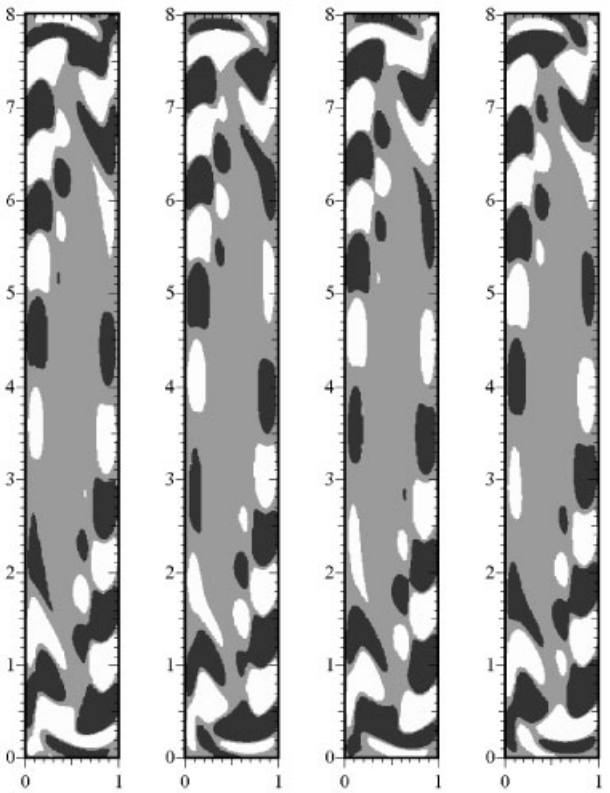

Figure 2. Plot of four captures of the perturbation of the temperature field during a complete period, $Ra = 3.4 \times 10^5$, non-dimensional time interval between captures 0.8517, $\Delta t = 10^{-3}$, grid resolution 30×120.

provides a measure of the skew-symmetry of the solution, this parameter being zero for skew-symmetric fields, and pressure differences $\Delta P_{14}, \Delta P_{51}$ and ΔP_{35}, defined by $\Delta P_{14} = P(0.181, 7.37) - P(0.819, 7.37)$, $\Delta P_{51} = P(0.181, 4) - P(0.181, 7.37)$ and $\Delta P_{35} = P(0.181, 0.63) - P(0.181, 4)$. All these statistics have been computed over 200 000 time steps, corresponding approximately to 58 periods and 3407 time steps per period. By increasing the spatial resolution, the period is found to converge to 3.4068. This value is however still affected by the time discretization error.

As the skewness values indicate, the solution obtained is skew-symmetric. Moreover, the analysis of the fluctuating fields of velocity, pressure and temperature shows the existence of 13 structures each made of two consecutive zones of positive and negative fluctuations.

Beside the spatial convergence, we checked also the time convergence, see Table V for the results. The convergence rate has been evaluated by the generalised theory of Richardson extrapolation [9]. Surprisingly, it turns out that the actual time accuracy is not second order but only first order. We have not been able to find an explanation for such a loss of accuracy of our spectral projection method.

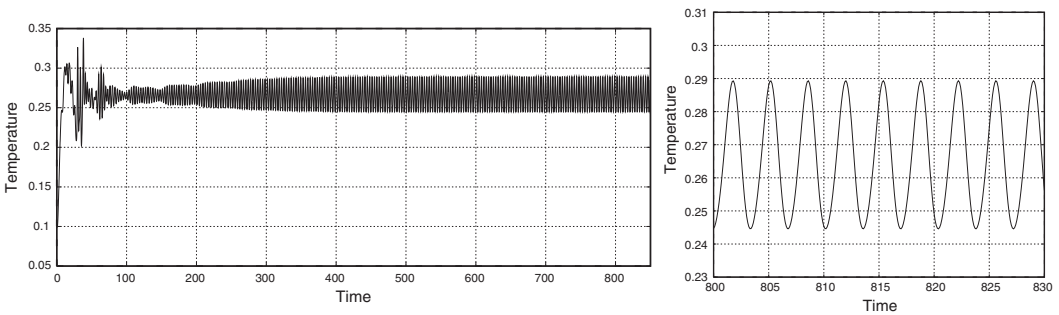

Figure 3. Evolution of the temperature point value at $(0.181, 7.370)$ (left) and particular of the asymptotic periodic behaviour (right), $Ra = 3.4 \times 10^5$.

Table III. Average values of point, wall and global quantities for the periodic solution, obtained by four different grid resolutions and $\Delta t = 10^{-3}$, $Ra = 3.4 \times 10^5$.

	Grid resolution			
Quantity	20×80	30×120	40×160	50×200
u	5.68065×10^{-2}	5.66994×10^{-2}	5.66998×10^{-2}	5.66700×10^{-2}
v	4.62051×10^{-1}	4.61862×10^{-1}	4.61864×10^{-1}	4.61865×10^{-1}
θ	2.65540×10^{-1}	2.65460×10^{-1}	2.65460×10^{-1}	2.65460×10^{-1}
ε	2.49247×10^{-15}	-1.87438×10^{-15}	-2.50133×10^{-16}	-3.63678×10^{-16}
ψ	-7.35656×10^{-2}	-7.35902×10^{-2}	-7.35901×10^{-2}	-7.35901×10^{-2}
ω	-2.34364	-2.35500	-2.35480	-2.35472
ΔP_{14}	-1.83181×10^{-3}	-1.84040×10^{-3}	-1.84036×10^{-3}	-1.84035×10^{-3}
ΔP_{51}	-5.34919×10^{-1}	-5.34909×10^{-1}	-5.35139×10^{-1}	-5.35140×10^{-1}
ΔP_{35}	5.36750×10^{-1}	5.34910×10^{-1}	5.34910×10^{-1}	5.34910×10^{-1}
$Nu_{x=0}$	-4.58518	-4.57967	-4.57952	-4.57951
$Nu_{x=W}$	-4.58518	-4.57967	-4.57952	-4.57951
$\hat{u}$	2.39582×10^{-1}	2.39571×10^{-1}	2.39570×10^{-1}	2.39570×10^{-1}
$\hat{\omega}$	3.01684	3.01690	3.01690	3.01690
T	3.4061	3.4068	3.4068	3.4068

3.2. *First Hopf bifurcation and following instabilities*

At $Ra = 3.4 \times 10^5$ the system has already gone through two bifurcations: the first at $Ra \approx 3.1 \times 10^5$ is of Hopf kind and the second one at $Ra \approx 3.15 \times 10^5$ is transcritical. As a matter of fact, it exists a first Hopf bifurcation which breaks the symmetry of the system, which is skew-symmetric about the centre of the cavity. Such a bifurcation can be observed, when employing a symmetry preserving numerical method as the present one, only if the computation is started from a non-symmetric initial field, as in the present computations.

Increasing the Rayleigh number, it is observed: a first instability which breaks the skew-symmetry of the flow at $Ra \approx 3.1 \times 10^5$, then, further increasing the Rayleigh number, a second

Table IV. Oscillation amplitude of point, wall and global quantities for the periodic solution, obtained by four different grid resolutions and $\Delta t = 10^{-3}$, $Ra = 3.4 \times 10^5$.

	Grid resolution			
Quantity	20×80	30×120	40×160	50×200
u	5.77611×10^{-2}	5.72417×10^{-2}	5.72434×10^{-2}	5.72427×10^{-2}
v	8.07758×10^{-2}	8.00311×10^{-2}	8.00313×10^{-2}	8.00314×10^{-2}
θ	4.51415×10^{-2}	4.47340×10^{-2}	4.47359×10^{-2}	4.47360×10^{-2}
ε	5.49560×10^{-15}	6.05071×10^{-15}	3.73034×10^{-14}	3.25572×10^{-14}
ψ	7.37788×10^{-3}	7.31321×10^{-3}	7.31349×10^{-3}	7.31352×10^{-3}
ω	1.14892	1.13089	1.13136	1.13139
ΔP_{14}	2.13713×10^{-2}	2.11906×10^{-2}	2.11913×10^{-2}	2.11915×10^{-2}
ΔP_{51}	2.34585×10^{-2}	2.32660×10^{-2}	2.32667×10^{-2}	2.32668×10^{-2}
ΔP_{35}	1.06351×10^{-2}	1.05369×10^{-2}	1.05373×10^{-2}	1.05373×10^{-2}
$Nu_{x=0}$	8.26308×10^{-3}	7.47329×10^{-3}	7.44177×10^{-3}	7.44198×10^{-3}
$Nu_{x=W}$	8.26308×10^{-3}	7.47329×10^{-3}	7.44177×10^{-3}	7.44198×10^{-3}
$\hat{u}$	3.50048×10^{-5}	3.46658×10^{-5}	3.46662×10^{-5}	3.46663×10^{-5}
$\hat{\omega}$	3.32555×10^{-3}	3.29997×10^{-3}	3.30006×10^{-3}	3.30010×10^{-3}

Table V. Oscillation amplitude versus Δt, grid resolution 30×120, $Ra = 3.4 \times 10^5$.

Δt	T_{P1}	$Nu_{x=0}$	$\hat{\omega}$
0.002	4.67590×10^{-2}	7.81688×10^{-3}	3.40635×10^{-3}
0.001	4.47340×10^{-2}	7.47329×10^{-3}	3.29997×10^{-3}
0.0005	4.37110×10^{-2}	7.29914×10^{-3}	3.24914×10^{-3}
0.0002	4.30942×10^{-2}	7.19395×10^{-3}	3.21526×10^{-3}

instability at $Ra \approx 3.15 \times 10^5$. Here the stable cycle which constitutes the asymptotic solution after the first bifurcation is superseded by another cycle with a larger frequency and a greater number of structures. Surprisingly enough, this second instability restores the lost skew-symmetry and it is probably the first to be observed by employing a symmetry preserving solver starting from a skew-symmetric initial condition. (See Figure 4).

The second instability seems to be an exchange of stability between lower- and higher-frequency solutions. The transcritical character of the instability is observed by looking at the temporal behaviour of the energy content of the relevant harmonics, namely the one associated with the 12 structure mode and the one associated with the 13 structure mode, reported in Figure 5. In fact, as shown in Figure 5 (left), for $Ra = 3.1 \times 10^5$ both modes are excited with a comparable initial amplitude, the lower-frequency mode amplifying with time while the higher-frequency mode decays. For $Ra = 3.15 \times 10^5$, a different behaviour is observed. As can be seen in Figure 5 (right), both modes start to grow, but for larger times the lower-frequency mode decays while the higher frequency one reaches an asymptote. An interesting feature that can be observed is also the energy exchange between the two modes which takes place at a frequency which is a fraction of the main frequencies, such an exchange tends to disappear as the system reaches its asymptotic status.

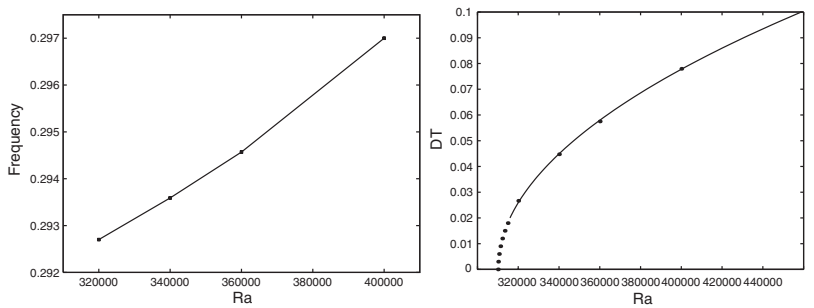

Figure 4. Frequency (left) and amplitude (right) versus Rayleigh between the second and third bifurcation points, $Ra = 3.4 \times 10^5$.

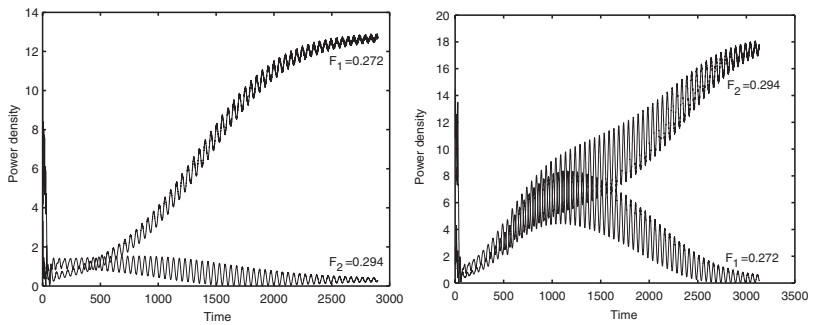

Figure 5. Time evolution of the power density for the two most energetic frequencies for $Ra = 3.1 \times 10^5$ (left) and $Ra = 3.15 \times 10^5$ (right).

As the Rayleigh number is further increased, two more bifurcations can be observed that lead to a periodic asymptotic behaviour. In each one the symmetry properties of the unsteady component of the solution change, so that while the perturbation after the first bifurcation is centro-symmetric, after the second bifurcation it is skew-symmetric. After the third bifurcation the perturbation does not have the skew-symmetry property nor the symmetry property, and after the fourth bifurcation it switches again to the skew-symmetry. The solution after the first bifurcation presents 12 structures, characterised by local temperature maxima and minima, and a frequency of 0.2724. After the second bifurcation the number of structures is increased to 13 and the frequency to 0.2936. The number of structures is increased further to 14, with a frequency of 0.3186, after the third bifurcation, located at $4.0 \times 10^5 < Ra \leqslant 4.5 \times 10^5$, and it increases further to 15 through the fourth bifurcation at $4.5 \times 10^5 < Ra \leqslant 5.0 \times 10^5$, the frequency growing to 0.3358. The discontinuous change of frequency going through the bifurcations is probably due to the increase of the number of structures. The appearance of the four asymptotic solutions can be observed in Figure 6, where snapshots of the temperature perturbation fields are reported.

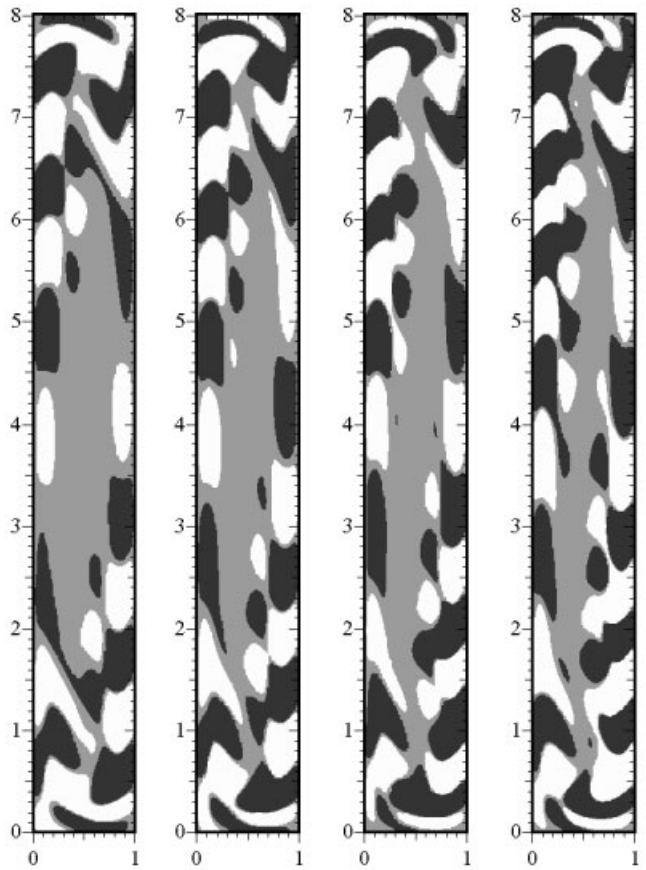

Figure 6. Instantaneous captures of temperature fluctuations. From left to right: $Ra = (3.1, 3.15, 4.5, 5.0) \times 10^5$.

4. CONCLUSIONS

A new spectral projection method for the simulation of natural convection in the Boussinesq approximation is proposed. The method relies on a Galerkin formulation and employs three different polynomial bases which are built by means of Legendre polynomials and which accommodate the different boundary conditions. The particular bases are formulated so that the maximum degree of sparsity in the discrete operators can be exploited in conjunction with the direct product structure of the problem. The projection scheme is an extension of the method proposed in Reference [7], and is formulated in pressure correction form with a second-order BDF time advancing scheme [2]. The spatial and temporal accuracy of the proposed method is thoroughly assessed by resorting to comparisons with both a problem with known analytical solution and established benchmark results [8].

The method is applied to the numerical investigation on the stability of natural convection in the differentially heated 8:1 cavity. In particular the first Hopf bifurcation has been located in the interval $3.075 \times 10^5 \leqslant Ra \leqslant 3.125 \times 10^5$. Moreover, three more transcritical bifurcations in

the range $3.15 \times 10^5 \leqslant Ra \leqslant 5.0 \times 10^5$ are recognized. The described sequence of bifurcations alternatively breaks and restores the skew-symmetry of the flow before the appearance of more complex dynamics for larger Rayleigh numbers. A detailed description of the solution at $Ra = 3.4 \times 10^5$ is also reported.

Finally, we must note that, while analytical tests assess the second order in time accuracy of the proposed method, a disappointing first-order convergence rate is achieved for the differentially heated cavity flow. The reason for this behaviour is not known, and therefore certainly deserves further investigation.

ACKNOWLEDGEMENTS

Special thanks are due to P. Le Quéré for his precious suggestions and to S. Xin for the helpful introduction to vectorial computing. All vector simulations were carried out on the NEC SX5 of IDRIS while the second author was visiting the Laboratoire d'lnformatique pour la Mécanique et les Sciences de l'lngénieur, Orsay. France, whose kind hospitality is sincerely acknowledged.

REFERENCES

1. Guermond JL, Quartapelle L. Calculation of incompressible viscous flows by an unconditionally stable projection FEM. *Journal of Computational Physics* 1997; **132**:12–33.
2. Guermond JL. Un résultat de convergence à l'ordre deux en temps pour l'approximation des équations de Navier–Stokes par une technique de projection. *Modélisation Mathématique et Analyse Numérique* 1999; **33**:169–189.
3. Paolucci S, Chenoweth DR. Transition to chaos in a differentially heated vertical cavity. *Journal of Fluid Mechanics* 1989; **201**:379–410.
4. Le Quéré P, Behnia M. From onset of unsteadiness to chaos in a differentially heated square cavity. *Journal of Fluid Mechanics* 1998; **359**:81–107.
5. Christon MA, Gresho PM, Sutton SB. Computational predictability of natural convection flows in enclosures. *International Journal for Numerical Methods in Fluids* 2002; **40**:953–980.
6. Shen J. Efficient spectral–Galerkin method. I. Direct solvers of second- and fourth-order equations using Legendre polynomials. *Society for Industrial and Applied Mathematics Journal on Scientific Computing* 1994; **15**: 1489–1505.
7. Auteri F, Parolini N. A mixed-basis spectral projection method. *Journal of Computational Physics* 2002; **175**: 1–23.
8. Le Quéré P. Accurate solutions to the square thermally driven cavity. *Computation of Fluids* 1991; **20**:29–41.
9. Roache PJ. Verification of Codes and Calculations. *American Institute of Aeronautics and Astronautics Journal* 1998; **36**:696–702.

